

Robust 3DGS-based SLAM via Adaptive Kernel Smoothing

Shouhe Zhang^{1,2}, Dayong Ren^{3,*}, Sensen Song^{1,2,*}, Wenjie Li⁴, Piaopiao Yu⁵ and Yurong Qian^{1,2}

¹School of Computer Science and Technology, Xinjiang University

²Joint International Research Laboratory of Silk Road Multilingual Cognitive Computing, Xinjiang University, Urumqi Xinjiang, 830046, China

³The National Key Laboratory for Novel Software Technology, Nanjing University

⁴Southwest University of Political Science and Law

⁵School of Computer Science and Technology, Nanjing University of Aeronautics and Astronautics, Nanjing 211106, China

Abstract—In this paper, we challenge the conventional notion in 3DGS-SLAM that rendering quality is the primary determinant of tracking accuracy. We argue that, compared to solely pursuing a perfect scene representation, it is more critical to enhance the robustness of the rasterization process against parameter errors to ensure stable camera pose tracking. To address this challenge, we propose a novel approach that leverages a smooth kernel strategy to enhance the robustness of 3DGS-based SLAM. Unlike conventional methods that focus solely on minimizing rendering error, our core insight is to make the rasterization process more resilient to imperfections in the 3DGS parameters. We hypothesize that by allowing each Gaussian to influence a smoother, wider distribution of pixels during rendering, we can mitigate the detrimental effects of parameter noise from outlier Gaussians. This approach intentionally introduces a controlled blur to the rendered image, which acts as a regularization term, stabilizing the subsequent pose optimization. While a complete redesign of the rasterization pipeline is an ideal solution, we propose a practical and effective alternative that is readily integrated into existing 3DGS frameworks. Our method, termed Corrective Blurry KNN (CB-KNN), adaptively modifies the RGB values and locations of the K-nearest neighboring Gaussians within a local region. This dynamic adjustment generates a smoother local rendering, reducing the impact of erroneous GS parameters on the overall image. Experimental results demonstrate that our approach, while maintaining the overall quality of the scene reconstruction (mapping), significantly improves the robustness and accuracy of camera pose tracking.

I. INTRODUCTION

Simultaneous Localization and Mapping (SLAM) is a cornerstone of robotics and computer vision, enabling autonomous agents to navigate unknown environments while concurrently constructing a map[1]. The field has seen remarkable advancements, particularly with the advent of real-time dense reconstruction methods[2]. Among these, the recent introduction of 3D Gaussian Splatting (3DGS) has garnered significant attention for its ability to render high-fidelity neural radiance fields at unprecedented speeds[3], [4], [5]. This paradigm shift from implicit neural representations to an explicit, point-based structure has opened new avenues for integrating rich scene representations directly into the SLAM loop[6]. Many modern 3DGS-based SLAM systems leverage this fast rasterization process, using the rendered depth and color images for photometric and geometric alignment to estimate camera pose[7], [8].

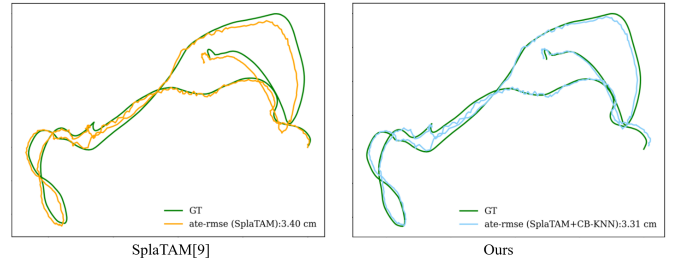


Fig. 1: In the fr1/desk scene of the TUM-RGBD[9] dataset, compared with the baseline(SpliTAM[10]) method, our method results in a smoother trajectory that is closer to the ground-truth trajectory.

Despite the promising real-time performance, we have identified a critical vulnerability in current 3DGS-based SLAM systems. The core challenge lies in the inherent inaccuracies of the high-dimensional Gaussian parameters[11], [12]. These parameters, which include position, orientation, scale, and color, are optimized from noisy camera observations[13], [14]. Consequently, the peripheral regions of the Gaussian kernels often contain significant errors. During the rasterization process, these erroneous parameters can lead to spurious artifacts in the rendered image, manifesting as incorrect pixel colors or even discontinuous holes in the scene[15]. These artifacts introduce substantial noise into the photometric alignment used for pose tracking, directly compromising the accuracy and robustness of the camera's localization, particularly in challenging conditions like fast motion or aggressive viewpoint changes[9], [16].

Traditional SLAM paradigms often operate under the assumption that a high-fidelity, visually sharp representation is essential for accurate pose estimation[17], [18], [19], [20]. However, in the context of 3DGS, we argue that this may not always be true. Our core insight is that for the purpose of pose tracking, a slightly smoother or blurred rendered image can be more resilient to the noise inherent in the Gaussian parameters[21]. We hypothesize that by enabling each Gaussian to influence a wider, more continuous region of pixels during rasterization, we can effectively regularize the rendering process[22]. This controlled smoothing effect dampens the impact of individual outlier Gaussians, produc-

ing a more stable and reliable image for subsequent pose optimization, thereby decoupling the requirements for scene fidelity and tracking robustness[21].

To realize this vision while remaining compatible with existing 3DGS frameworks, we propose Corrective Blurry KNN (CB-KNN), a novel and practical approach for adaptive kernel smoothing. We recognize that while a complete redesign of the rasterization pipeline would be ideal, it is both complex and lacks the flexibility needed for real-world applications with evolving technology and mobile computing constraints[23]. Instead, our CB-KNN method acts as a dynamic correction mechanism that can be seamlessly integrated into existing pipelines. Its core idea is to introduce a local neighborhood-based smoothing term when calculating each pixel's value. Specifically, for a given pixel, the rasterizer identifies the K-nearest neighboring Gaussians and applies an on-the-fly adjustment to their parameters[24], [23]. This adjustment involves correcting their locations by subtly shifting them towards their collective centroid, effectively creating a more cohesive overlap in the 2D image plane and filling in gaps caused by parameter errors[25]. Concurrently, we correct their RGB values by computing a weighted average, which prevents individual outlier Gaussians from introducing color noise and improves the overall noise resistance of the rendered image[1].

It is crucial to emphasize that these corrections are transient and do not permanently alter the underlying 3DGS map parameters[1]. This temporary smoothing acts as a form of regularization, enabling us to enhance pose tracking robustness without compromising the integrity of the scene representation[2], [3]. Furthermore, to address the high computational cost of large-scale SLAM, our CB-KNN method is strategically applied only to keyframes during the mapping stage[6]. As keyframes are fundamental to map construction and pose accuracy[8], ensuring a robust and stable rendering from these critical views provides a strong foundation for all subsequent tracking[26]. This selective application allows our approach to achieve outstanding tracking accuracy and robustness while remaining computationally feasible for real-world mobile scenarios.

The key contributions of this work are as follows:

- 1) We introduce a novel perspective for 3DGS-based SLAM, shifting the focus from maximizing visual fidelity to ensuring the robustness of pose estimation.
- 2) We propose the concept of adaptive kernel smoothing to mitigate the detrimental effects of parameter noise on the rasterized image.
- 3) We present Corrective Blurry KNN (CB-KNN), a practical and effective method that can be seamlessly integrated into existing 3DGS frameworks.
- 4) We provide comprehensive experimental results demonstrating that our approach significantly improves tracking accuracy and robustness while preserving mapping quality.

II. RELATED WORK

A. 3D Gaussian Splatting Technique

The 3D Gaussian Splattering[1] technique breaks through the real-time rendering bottleneck of NeRF's[4], [27], [28], [29], [30] implicit representation, enabling high-fidelity, millisecond-level rendering through an explicit set of high-dimensional Gaussians. This constitutes its core advantage. However, most subsequent studies have focused on rendering clarity, neglecting the impact of Gaussian parameter errors on downstream pose estimation. This issue becomes prominent when 3DGS is integrated with SLAM, forming the core of this research.

B. Research on SLAM Systems Using 3D Gaussian Splatting

In research on 3DGS-based SLAM systems[3], [31], [32], [33], [34], [35], a closed loop of map construction-rendering alignment-pose estimation is established, utilizing rapidly rendered rapidly rendered color maps and depth maps to achieve pose tracking. During rapid camera movement or drastic view changes[36], rendering artifacts can cause photometric alignment failure, leading to pose drift or even loss[32]. This deficiency demonstrates that existing systems fail to decouple scene fidelity from tracking robustness, highlighting the necessity of redesigning 3DGS rendering strategies.

C. Robustness Optimization Methods for SLAM Pose Tracking

Traditional SLAM robustness strategies, such as ORB-SLAM3[11], eliminate outliers through dynamic weighting of feature points and suppress abnormal errors using robust losses and kernel functions. However, these methods are designed specifically for observation noise and do not account for parameter errors in 3DGS or alignment noise caused by rendering artifacts[1], [32]. For 3DGS-based SLAM systems[3], [31], [32], [33], [34], [35], noise originates from map representation errors[37], [38], making traditional methods ineffective in addressing the problem at its source. Instead, active regularization must be applied during the rendering process, which fundamentally distinguishes our approach from the kernel smoothing strategy proposed in this paper.

D. Application of Kernel Smoothing Techniques in Vision and SLAM

Kernel smoothing achieves data regularization through weighted averaging of local neighborhoods[37], [39]. However, existing studies either target 2D pixels[40], operate on 3D point clouds[41], [28], [29], [30], [42], [43], [44], or are confined to the data association stage of SLAM[37], without involving regularization in the 3DGS rendering process. The CB-KNN method proposed in this paper is characterized by three aspects: first, designing dynamic correction in both position and RGB dimensions for the explicit representation of 3DGS; second, employing kernel smoothing as a temporary regularization term in rendering without modifying the underlying map; and third, applying it only to keyframes

to control computational costs. These three aspects fill the gap in the application of kernel smoothing in 3D Gaussian splatting.

III. METHOD

This section systematically elaborates the integration implementation process of 3D Gaussian Splatting (3DGS)[1] and Simultaneous Localization and Mapping (SLAM) by incorporating the Corrective Blurry K-Nearest Neighbors (Corrective Blurry KNN,CB-KNN) adaptive kernel kernel smoothing strategy. Our design consistently adheres to three core principles: temporary rendering correction – keyframe smoothing – original map fidelity, ensuring the suppression of Gaussian parameter errors while maintaining compatibility with existing 3DGS differentiable rendering and SLAM pose optimization. The overall workflow of the proposed method is illustrated in Fig.2.

A. Gaussian Representation and Differentiable Rendering.

Using a 3D Gaussian set as the explicit scene representation, the robustness of the rendering process is optimized through the CB-KNN correction mechanism, while preserving the differentiable property of 3DGS to support end-to-end pose and map optimization. This subsection is elaborated from three dimensions: Gaussian parameter definition, rendering pipeline design, and image generation.

3D Gaussian Map Representation. We represent the scene on the map using a set of 3D Gaussians $G = \{g_1, g_2, \dots, g_N\}$. A single Gaussian is denoted as $g_i = (u_i, \sigma_i, r_i, c_i)$, where $u_i \in \mathbb{R}^3$ represents the center position of the Gaussian; $\sigma_i \in [0, 1]$ denotes the opacity; r_i represents the Gaussian radius; and c_i denotes the view-independent RGB color. Here, we use view-independent colors to satisfy the isotropy of the Gaussian distribution. We still adopt the radial decay function of the Gaussian distribution proposed in the literature[1]:

$$f(x) = \sigma_i \cdot \exp\left(-\frac{\|x - \mu_i\|_i^2}{r_i^2}\right). \quad (1)$$

All Gaussian parameters $(u_i, \sigma_i, r_i, c_i)$ in the map are referred to as original parameters. In subsequent CB-KNN correction, modifications are only applied to the temporary parameters during the rendering phase, without retroactively altering the original map.

CB-KNN-Enhanced Differentiable Rendering. Our method differentiably renders color, depth, and contour images from Gaussian maps at the CUDA level into any possible camera reference frame. It also renders Gaussian distributions into 2D images[1], [10]. During this process, we integrate CB-KNN correction into the Gaussian filtering-pixel calculation stage to obtain rendering results smoothed by CB-KNN, including RGB maps, depth maps, and contour maps. The procedure is as follows: first, we filter visible Gaussians for the current frame through frustum culling and sort them by camera distance; second, we select neighboring Gaussians, specifically choosing the K nearest Gaussians that contribute the most to each pixel $p = (u, v)$, denoted

as $G_P = \{g_{p1}, g_{p2}, \dots, g_{pK}\}$ (where K is a adaptive kernel parameter, detailed in Adaptive Selection of K value in CB-KNN); third, we perform CB-KNN temporary correction by adjusting the positions (means3D) and colors (rgb colors) of G_P to generate a temporary Gaussian set G'_P ; finally, we conduct image rendering to generate RGB maps, depth maps, and contour maps based on G'_P . It should be noted that all corrections only affect the current frame rendering and do not update the original Gaussians G .

B. Rendering Formula Optimization (Incorporating CB-KNN Correction)

We have incorporated the CB-KNN correction and presented the rendering formulas for each image, emphasizing the regularization effect of controllable smoothing.

RGB Image Rendering. For a pixel $p = (u, v)$, the rendered color corresponds to the alpha compositing of corrected Gaussian colors, where the formula integrates temporary RGB corrections and the original attenuation function[1]:

$$C(p) = \sum_{g_{pk} \in G'_P} c'_{pk} \cdot f_{pk}(p) \cdot \prod_{j=1}^{k-1} (1 - f_{pj}(p)). \quad (2)$$

Herein, c'_{pk} denotes the Gaussian color corrected by CB-KNN (detailed in Color Correction (Weighted Smoothing)); $f_{pk}(p)$ represents the attenuation value of the corrected Gaussian at pixel p (consistent with Equation (1), taking the corrected 2D projection position as input); the product term corresponds to forward transparency accumulation, ensuring consistency in rendering order.

Depth Image Rendering. The depth value is determined as the weighted average of corrected Gaussian depths[10], with weights derived from the Gaussian attenuation function. The calculation method is as follows:

$$D(p) = \sum_{g_{pk} \in G'_P} d'_{pk} f_{pk}(p) \cdot \prod_{j=1}^{k-1} (1 - f_{pj}(p)). \quad (3)$$

Herein, d'_{pk} represents the depth of the corrected Gaussian in the camera coordinate system. This formula enables depth smoothing, mitigates depth discontinuities caused by anomalous Gaussians, and simultaneously returns gradients relative to the original 3D map to facilitate pose optimization.

Contour Image Rendering. For the calculation method of contour image rendering, we adopt the contour computation approach from SplaTAM[10], with the input replaced by the corrected Gaussian set to ensure the accuracy of visibility judgment:

$$S(p) = \sum_{g_{pk} \in G'_P} f_{pk}(p) \cdot \prod_{j=1}^{k-1} (1 - f_{pj}(p)). \quad (4)$$

The value of $S(p)$ closer to 1 indicates a more complete Gaussian coverage of pixel p , resulting in a higher weight assigned to this pixel in subsequent pose optimization.

Calculation Method for CB-KNN Smoothing Correction. Based on the K-nearest neighbor smoothing logic

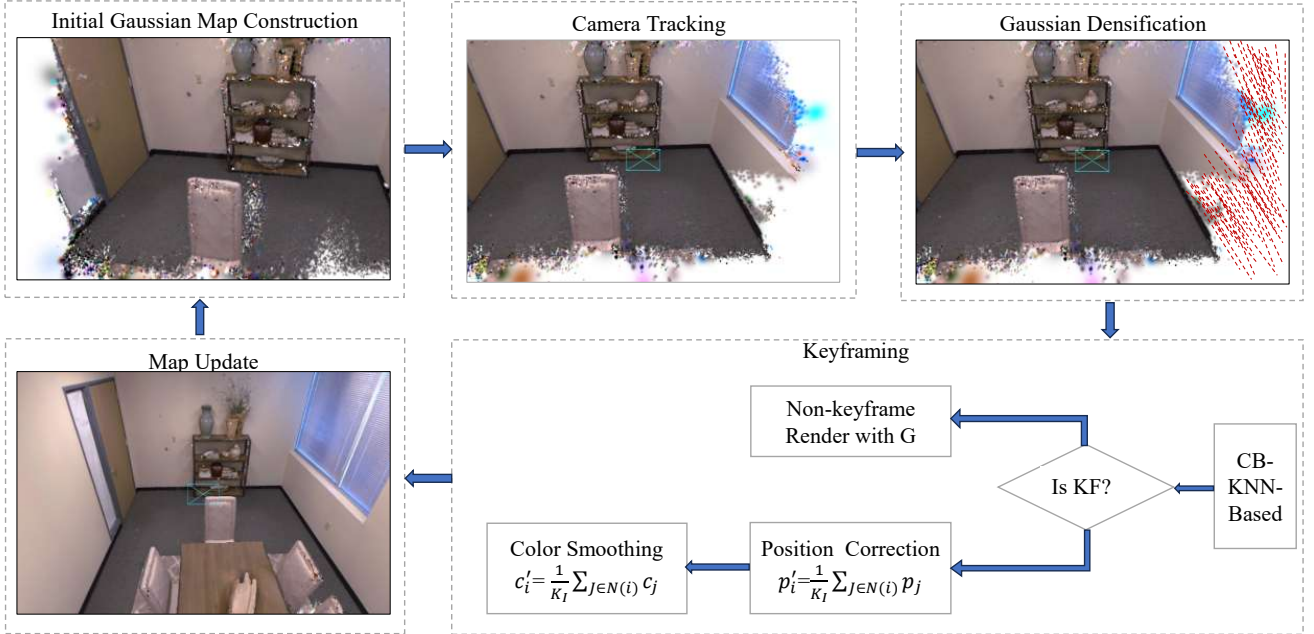


Fig. 2: The flowchart illustrates the workflow of a 3DGS - SLAM method based on CB - KNN. It starts with initial Gaussian map construction, proceeds through camera tracking and Gaussian densification, then keyframing (where keyframes undergo CB - KNN - based position correction and color smoothing), and finally map update, forming a complete SLAM cycle.

proposed in this work, we extend it to dual-dimensional correction of position and color. In the following, we elaborate on the calculation method for CB-KNN smoothing correction. For each Gaussian g_{pk} in G_p , we first compute the 2D projection centroid C_p of the K nearest neighbors:

$$C_p = \frac{1}{K} \sum_{g_{pj} \in G_p} \pi(\mu_{pj}, E_t, K_{cam}). \quad (5)$$

Herein, $\pi(\cdot)$ denotes the 3D-to-2D projection function, which takes the Gaussian 3D position u_{pj} , camera extrinsic parameters E_t , and camera intrinsic parameters K_{cam} as inputs. The position correction (2D projection offset) is then obtained by shifting the 2D projection of g_{pk} toward C_p :

$$\pi(\mu'_{pk}) = \pi(\mu_{pk}) + \alpha \cdot \frac{C_p - \pi(\mu_{pk})}{\|C_p - \pi(\mu_{pk})\| + \varepsilon}. \quad (6)$$

Herein, $\alpha \in [0.1, 0.3]$ represents the offset coefficient, $\varepsilon = 10^{-6}$ is introduced to avoid division by zero, and u'_{pk} denotes the temporarily corrected 3D position (used solely for current frame rendering). Weights are assigned based on the contribution of each Gaussian to pixel p , yielding the corrected color as follows:

$$c'_{pk} = \sum_{g_{pj} \in G_p} \omega_{pj} \cdot c_{pj}, \quad \omega_{pj} = \frac{f_{pj}(p)}{\sum_{g_{pj} \in G_p} f_{pj}(p)}. \quad (7)$$

Herein, ω_{pj} represents the normalized weight, which guarantees that Gaussians with higher contribution take precedence in color determination while suppressing color noise induced by anomalous Gaussians.

C. CB-KNN-based SLAM System

With the logical framework of taking original map optimization as the foundation, temporary correction of keyframes as the core, and tracking of non-keyframes as a supplement, the CB-KNN correction is embedded into the SLAM pipeline. This framework clarifies the input-output relationships, parameter update rules, and anomaly handling mechanisms for each stage. In the following, we detail the implementation of our CB-KNN-based SLAM system.

Initial Map Construction. We initialize the 3D Gaussian map using RGB-D images from frame 1 to frame t . All pixels in the first frame are back-projected into initial Gaussians, and the original Gaussian parameters G are optimized iteratively by minimizing RGB and depth errors through differentiable rendering. For the RGB-D image of frame $t + 1$, which represents new sensory input, we perform camera tracking, Gaussian densification, and map updating to complete the processing of this frame. As these constitute the core tasks of SLAM, the detailed procedures are elaborated as follows.

Camera Tracking. Camera tracking is inherently intertwined with image frame processing. We categorize image frame processing into two types: non-keyframe tracking and keyframe correction optimization. For non-keyframe tracking, where the core requirement is fast camera pose estimation, CB-KNN correction is not performed. Instead, RGB and depth maps are directly rendered using the original Gaussians G , and the pose is optimized by minimizing rendering errors with initialization based on a constant-velocity model ($E_{t+1} = E_t + (E_t - E_{t-1})$). Keyframes are crucial for map

updates and pose accuracy, requiring CB-KNN correction to enhance rendering robustness and provide reliable foundations for subsequent pose tracking and map optimization. For keyframe correction optimization: we first perform pixel-level K-nearest neighbor Gaussian selection G_p based on the original Gaussians G ; then apply position (means3D) and color (rgb colors) corrections to G_p to generate a temporary set G'_p ; next, obtain smoothed RGB, depth, and contour maps through rendering based on G'_p ; finally, we optimize the pose by minimizing the loss function using these smoothed images as inputs. The loss function employed for minimization is:

$$L_t = \sum_{p:S(p)>0.99} (L_1(D(p) - D_{GT}(p)) + 0.6L_1(C(p) - C_{GT}(p))). \quad (8)$$

Herein, $D_{GT}(p)$ and $C_{GT}(p)$ denote the ground-truth depth and color of the input RGB-D frame, respectively. The color weight of 0.6 is determined as the optimal value through repeated experiments. The constraint $S(p) > 0.99$ ensures that only pixels with complete coverage are used for loss calculation, thereby enhancing robustness.

Gaussian Densification. For the implementation of Gaussian densification, we employ the methodology proposed in SplatAM[10]. The primary objective of Gaussian densification is to initialize new Gaussian distributions within the map upon the arrival of new input data. Leveraging the tracked camera poses, we generate a densification mask to identify regions exhibiting insufficient density (contour mask < 0.5) or containing novel geometric structures (where ground-truth depth lies ahead of the predicted depth with an error surpassing the predefined threshold). New Gaussian distributions are introduced in these identified regions, adhering to the same parameter initialization protocol as applied to the first frame. In this context, we utilize the densification mask computation method from SplatAM[10] to determine which pixels require densification:

$$M(p) = (S(p) < 0.5) + (DGT(p) < D(p)) (L1(D(p)) > \lambda MDE). \quad (9)$$

Herein, λ denotes the error threshold, which is set to 50 in our implementation, MDE represents the median depth error.

CB-KNN-based Keyframe Selection. The core function of keyframes is to provide an optimization basis for map updates. We adopt the following approach for keyframe selection: frames are selected and stored from continuously input RGB-D sequences, with every n th frame saved as a keyframe. Herein, keyframes undergo CB-KNN processing, which is exclusively applied to keyframes while non-keyframes retain original rendering, thereby reducing computational costs. This is specifically manifested in: smoothing the 3D point cloud back-projected from depth maps to calculate the overlap between keyframes and the current frame (determined by counting points within each keyframe's viewing frustum from the point cloud of the current frame's depth map), which enhances the accuracy of overlap calculation. Through CB-KNN-based smoothing of keyframes, we

enable more stable criteria for selecting keyframes for map updates, achieving the goal of more precise mapping.

Adaptive Selection of K value in CB-KNN. The K value (number of neighboring Gaussians) is jointly determined by local Gaussian density and scene complexity. For local density calculation, the keyframe image is divided into an 8×8 pixel grid, and the number of Gaussian projections within each grid, denoted as D , is counted. The density is defined as $\rho = D/64$ (where 64 pixels represent the grid area). For scene complexity evaluation, the motion amplitude between adjacent keyframes is normalized to obtain $\gamma \in [0, 1]$ (with $\gamma = 1$ indicating maximum motion). Thus, the calculation method for the K value in CB-KNN is given by:

$$K = K_0 \cdot \max \left(0.5, 1 - \beta \cdot \frac{\gamma}{\rho + \epsilon} \right). \quad (10)$$

Herein, the baseline value $K_0 = 8$ and the adjustment coefficient $\beta = 0.3$. Due to variations in Gaussian density and scene complexity across different scenarios, increasing the K value enhances the smoothing effect when Gaussian density is low or scene complexity is high; conversely, decreasing the K value preserves scene details.

Map Update. During the map update phase, we utilize the poses of all keyframes (including the current keyframe) and employ CB-KNN to optimize all Gaussian parameters G . Selected keyframes, comprising the current frame, the latest keyframe, and the top $k - 2$ keyframes with the highest overlap with the current frame, undergo CB-KNN correction. Through differentiable rendering, we minimize RGB errors (including SSIM loss) and depth errors; simultaneously, invalid Gaussian distributions with opacity approaching 0 or excessively large dimensions are pruned. This completes the map update process.

IV. EXPERIMENT

A. Experimental Setup

Datasets. Our method is evaluated on both synthetic and real-world datasets, including 8 scenes from Replica[16], 3 scenes from TUM-RGBD[9], and 4 scenes from the original ScanNet[45]. For our SLAM system, the localization metrics follow those used in previous radiance field-based SLAM approaches, specifically employing the average absolute trajectory error (ATE RMSE [cm]) to assess localization accuracy. For mapping performance, we use the average depth L1 to evaluate tracking precision. For image rendering quality assessment, metrics including Peak Signal-to-Noise Ratio (PSNR[dB]), Structural Similarity Index (SSIM), and Learned Perceptual Image Patch Similarity (LPIPS) are adopted. For the Replica[16], which represents the simplest benchmark containing synthetic scenes, highly accurate and complete (synthetic) depth maps, along with minimal displacements between consecutive camera poses, we apply CB-KNN-based smoothing to 3D point coordinates, RGB colors, and keyframes with $K_0 = 5$. For the TUM-RGBD[9] and original ScanNet[45], which utilize older low-quality cameras resulting in poor RGB and depth image quality, highly sparse depth maps with significant information loss,

and severe motion blur in color images, we employ CB-KNN-based smoothing to 3D point coordinates, RGB colors, and keyframes with $K_0 = 8$.

B. Evaluation of SLAM Metrics

In terms of SLAM metric evaluation, the primary baseline(SplaTAM[10]) method against which we compare is SplaTAM[10], which represents a state-of-the-art approach in previous 3D Gaussian splatting-based SLAM.

Tracking performance evaluation. For evaluating the localization performance of our SLAM system, we conducted the following experiments on three datasets. As shown in TABLE I , on the Replica[16], we additionally included another 3D Gaussian splatting-based SLAM method: MonoGS[2] for comparison. Our SLAM method reduces the ATE RMSE from 0.39 cm to 0.32 cm compared with the baseline(SplaTAM[10]) method, achieving the best performance;on the TUM-RGBD[9], our SLAM method reduces the ATE RMSE from 3.31 cm to 3.18 cm compared with the SplaTAM[10] method, achieving the best performance;on the ScanNet[45], our SLAM method demonstrates the best performance on scene 0181. Compared with the SplaTAM[10] method, our SLAM method has certain advantages, reducing the ATE RMSE from 13.43 cm to 12.48 cm.

Relative Pose Error Analysis. To verify the effectiveness of the proposed CK-KNN method for local data, a relative pose error experiment was conducted, yielding the relative pose error (RPE[cm]). In TABLE II, for the eight scenes in the Replica[16], 50 frames with significant focal length variations were selected from each scene for testing. For the TUM-RGBD[9] and ScanNet[45], the same frame selection method as that used for the Replica[16] was adopted, with 100 frames selected for testing. From the experimental results, our CK-KNN method is effective and outperforms the SplaTAM[10] method.

Rendering Performance Evaluation. In TABLE III, on the Replica dataset, the rendering performance of our SLAM system is comparable to that of the SplaTAM[10] method. Among them, our method achieves the best result in terms of LPIPS, with a value of 0.09, outperforming all other approaches. On the TUM-RGBD[9], compared with the SplaTAM[10] method, our SLAM approach improves the PSNR from 22.80 dB to 23.87 dB. On the ScanNet[45], our SLAM method shows improvements in all rendering quality metrics compared to the SplaTAM[10] method. While Point-SLAM[34] demonstrates superior reconstruction performance on the Replica dataset due to its use of ground-truth point cloud inputs, our method outperforms it on the core task of tracking.

Rendering performance of novel view and training view. In TABLE IV, we conducted novel view and training view rendering experiments on the R0 within the Replica[16] and evaluated their performance. The rendering results are presented in Fig.3.

C. Runtime Comparison

In TABLE V, for Replica/R0, we compared our runtime with SplaTAM[10] using an NVIDIA A40. In contrast to

SplaTAM[10], in TABLE VI, we additionally report the average frame rate (FPS) and the time for optimizing keyframes (Keyframe time), where our keyframe optimization employs CB-KNN. Consistent with SplaTAM[10], 40 and 60 iterations are used for per-frame tracking and mapping, respectively.

D. Trajectory Analysis

From the trajectories of the R1 and Of1 scenes in the Replica[16], it can be observed that the trajectory of our SLAM method achieves complete alignment with the ground-truth trajectory. For the trajectories of the fr1/desk and fr3/off. scenes in the TUM-RGBD[9], as well as the scene0106 and scene0207 scenes in the ScanNet[45], compared with the SplaTAM[10] method, the trajectory of our SLAM method is smoother and closer to the ground-truth trajectory. The trajectory maps are presented in Fig.4.

V. CONCLUSIONS

In this paper, we present a novel 3DGS-SLAM method that enhances robustness through an adaptive kernel smoothing strategy. We challenge the conventional wisdom that perfect visual fidelity is the primary determinant of tracking accuracy, demonstrating that a controlled rendering regularization effectively mitigates the impact of 3DGS parameter noise on pose tracking. Our core contribution is Corrective Blurry KNN (CB-KNN), a method that dynamically adjusts Gaussian parameters in local regions to produce a regularization effect during rendering, without altering the underlying map parameters. For computational efficiency, this strategy is applied only to keyframes. Experimental results demonstrate that our method significantly improves the accuracy and stability of pose tracking while maintaining high-quality map reconstruction.

REFERENCES

- [1] Bernhard Kerbl, Georgios Kopanas, Thomas Leimkühler, and George Drettakis, “3d gaussian splatting for real-time radiance field rendering,” *ACM Trans. Graph.*, vol. 42, no. 4, pp. 139–1, 2023.
- [2] Hidenobu Matsuki, Riku Murai, Paul HJ Kelly, and Andrew J Davison, “Gaussian splatting slam,” in *Proceedings of the IEEE/CVF Conference on Computer Vision and Pattern Recognition*, 2024, pp. 18039–18048.
- [3] Chi Yan, Delin Qu, Dan Xu, Bin Zhao, Zhigang Wang, Dong Wang, and Xuelong Li, “Gs-slam: Dense visual slam with 3d gaussian splatting,” in *Proceedings of the IEEE/CVF Conference on Computer Vision and Pattern Recognition*, 2024, pp. 19595–19604.
- [4] Kyle Gao, Yina Gao, Hongjie He, Dening Lu, Linlin Xu, and Jonathan Li, “Nerf: Neural radiance field in 3d vision, a comprehensive review,” *arXiv preprint arXiv:2210.00379*, 2022.
- [5] Feifei Zhang, Fei Shi, Dayong Ren, and Yue Li, “A fuzzy c-means clustering algorithm for real medical image segmentation,” in *ICASSP 2025-2025 IEEE International Conference on Acoustics, Speech and Signal Processing (ICASSP)*. IEEE, 2025, pp. 1–5.
- [6] Alex Yu, Ruilong Li, Matthew Tancik, Hao Li, Ren Ng, and Angjoo Kanazawa, “Plenoctrees for real-time rendering of neural radiance fields,” in *Proceedings of the IEEE/CVF international conference on computer vision*, 2021, pp. 5752–5761.
- [7] Kara-Ali Aliev, Artem Sevastopolsky, Maria Kolos, Dmitry Ulyanov, and Victor Lempitsky, “Neural point-based graphics,” in *European conference on computer vision*. Springer, 2020, pp. 696–712.
- [8] Qingtian Zhu, Zizhuang Wei, Zhongtian Zheng, Yifan Zhan, Zhuyu Yao, Jiawang Zhang, Kejian Wu, and Yinqiang Zheng, “Rpbg: Towards robust neural point-based graphics in the wild,” in *European Conference on Computer Vision*. Springer, 2024, pp. 389–406.

TABLE I: The tracking performance on Replica[16], TUM-RGBD[9], and ScanNet[45] (ATE RMSE↓[cm])

Dataset		Replica[16]									TUM-RGBD[9]				ScanNet[45]				
Methods	Avg.	R0	R1	R2	Of0	Of1	Of2	Of3	Of4	Avg.	fr1/desk	fr2/xyz	fr3/off	Avg.	0000	0106	0169	0181	
Vox-Fusion[36]	3.09	1.37	4.70	1.47	8.48	2.04	2.58	1.11	2.94	10.34	3.52	1.49	26.01	31.96	68.84	8.41	27.28	23.30	
NICE-SLAM[35]	1.07	0.97	1.31	1.07	0.88	1.00	1.06	1.10	1.13	6.87	4.26	31.73	3.87	11.05	12.00	7.90	10.90	13.40	
ESLAM[33]	0.63	0.71	0.70	0.52	0.57	0.55	0.58	0.72	0.63	2.00	2.47	1.11	2.42	—	—	—	—	—	
Co-SLAM[31]	1.06	0.72	0.85	1.02	0.69	0.56	2.12	1.62	0.87	2.17	2.40	1.70	2.40	—	—	—	—	—	
Point-SLAM[34]	0.52	0.61	0.41	0.37	0.38	0.48	0.54	0.69	0.72	3.48	4.34	1.31	3.48	13.96	10.24	8.65	22.16	14.77	
MonoGS[2]	0.79	0.47	0.43	0.31	0.70	0.57	0.31	0.31	3.20	1.47	1.50	1.44	1.49	—	—	—	—	—	
SplaTAM[10]	0.39	0.31	0.40	0.36	0.53	0.27	0.29	0.32	0.64	3.31	3.40	1.36	5.16	13.43	12.83	17.72	12.08	11.10	
Ours	0.32	0.25	0.34	0.27	0.42	0.21	0.27	0.33	0.52	3.18	3.31	1.34	4.90	12.48	11.64	17.64	11.91	8.74	

TABLE II: The Relative Pose Error (RPE↓[cm]) on Replica[16], TUM-RGBD[9], and ScanNet[45]

Dataset		Replica[16]									TUM-RGBD[9]				ScanNet[45]				
Methods	Avg.	R0	R1	R2	Of0	Of1	Of2	Of3	Of4	Avg.	fr1/desk	fr2/xyz	fr3/off	Avg.	0000	0106	0169	0181	
SplaTAM[10]	0.10	0.14	0.09	0.08	0.04	0.06	0.07	0.15	0.18	1.58	1.35	0.98	2.42	1.47	1.10	1.08	2.03	1.68	
Ours	0.08	0.12	0.08	0.05	0.04	0.05	0.06	0.12	0.10	1.48	1.30	0.90	2.25	1.35	1.08	1.00	1.83	1.50	

TABLE III: The rendering performance on Replica[16], TUM-RGBD[9], and ScanNet[45]

Dataset		Replica[16]									TUM-RGBD[9]				ScanNet[45]				
Methods	Metrics	Avg.	R0	R1	R2	Of0	Of1	Of2	Of3	Of4	Avg.	fr1/desk	fr2/xyz	fr3/off	Avg.	0000	0106	0169	0181
Vox-Fusion[36]	PSNR↑	24.41	22.39	22.36	23.92	22.36	29.83	20.33	23.47	25.21	16.46	15.79	16.32	17.27	18.17	19.06	18.46	18.69	16.75
	SSIM↑	0.80	0.68	0.75	0.80	0.75	0.88	0.79	0.80	0.85	0.65	0.65	0.65	0.65	0.68	0.66	0.75	0.65	0.67
	LPIPS↓	0.24	0.30	0.27	0.23	0.27	0.18	0.24	0.21	0.20	0.47	0.52	0.43	0.46	0.50	0.52	0.44	0.51	0.53
NICE-SLAM[35]	PSNR↑	24.42	22.12	22.47	24.52	22.47	30.34	19.66	22.23	24.96	14.86	13.83	17.87	12.89	17.85	18.71	18.75	15.56	18.38
	SSIM↑	0.81	0.69	0.76	0.81	0.76	0.89	0.80	0.80	0.86	0.61	0.57	0.72	0.55	0.62	0.64	0.65	0.63	0.56
	LPIPS↓	0.23	0.33	0.27	0.21	0.27	0.18	0.24	0.21	0.20	0.44	0.48	0.34	0.50	0.55	0.56	0.51	0.53	0.60
ESLAM[33]	PSNR↑	28.06	25.25	27.39	28.09	27.39	27.04	27.99	29.27	29.15	15.26	11.29	17.46	17.02	14.98	15.70	15.44	14.56	14.22
	SSIM↑	0.92	0.87	0.89	0.94	0.89	0.91	0.94	0.95	0.95	0.48	0.67	0.31	0.46	0.67	0.69	0.63	0.66	0.70
	LPIPS↓	0.26	0.32	0.30	0.25	0.30	0.25	0.24	0.21	0.21	0.57	0.36	0.70	0.65	0.63	0.45	0.53	0.49	0.48
Point-SLAM[34]	PSNR↑	35.17	32.40	34.08	35.50	34.08	39.16	33.99	34.48	33.49	16.62	13.87	17.56	18.43	19.73	21.30	16.80	18.53	22.27
	SSIM↑	0.98	0.97	0.98	0.98	0.98	0.96	0.96	0.98	0.95	0.70	0.63	0.71	0.75	0.75	0.81	0.67	0.69	0.82
	LPIPS↓	0.12	0.11	0.12	0.11	0.12	0.12	0.16	0.13	0.14	0.53	0.54	0.59	0.45	0.51	0.49	0.54	0.54	0.47
SplaTAM[10]	PSNR↑	34.11	32.86	33.89	35.25	33.89	39.17	31.97	29.70	31.81	22.80	22.00	24.50	21.90	18.54	18.58	17.73	21.52	16.33
	SSIM↑	0.97	0.98	0.97	0.98	0.97	0.98	0.97	0.95	0.95	0.89	0.86	0.95	0.88	0.70	0.66	0.69	0.78	0.68
	LPIPS↓	0.10	0.07	0.10	0.08	0.10	0.09	0.10	0.12	0.15	0.18	0.23	0.10	0.20	0.38	0.44	0.38	0.28	0.42
Ours	PSNR↑	34.17	32.66	33.58	35.11	33.58	39.48	32.00	30.14	32.04	23.87	24.41	25.30	21.93	19.14	19.23	18.28	21.93	17.12
	SSIM↑	0.97	0.98	0.97	0.98	0.97	0.98	0.97	0.95	0.95	0.92	0.92	0.95	0.88	0.71	0.66	0.71	0.78	0.70
	LPIPS↓	0.09	0.05	0.10	0.07	0.10	0.09	0.10	0.11	0.15	0.15	0.16	0.09	0.21	0.33	0.38	0.33	0.25	0.38

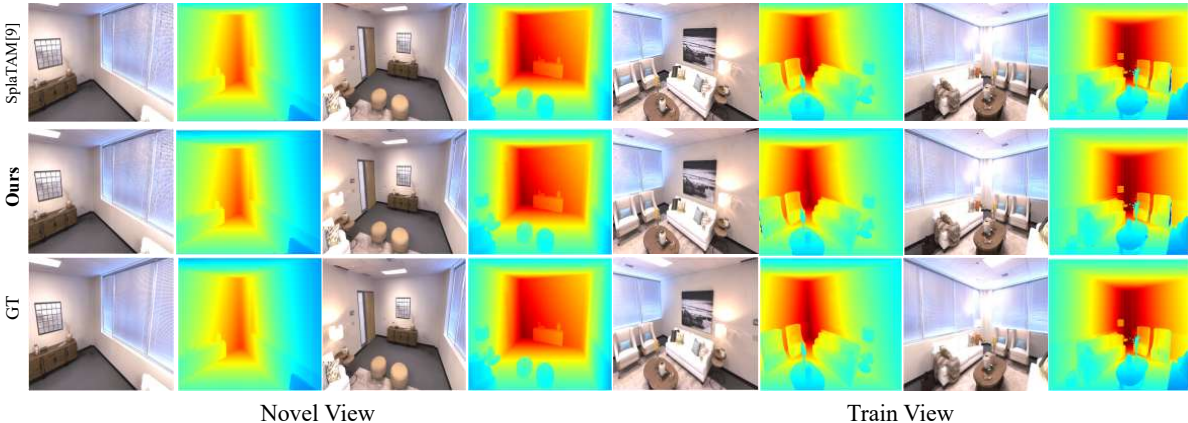


Fig. 3: Rendering results on the Room0 from Replica[16]. It can be observed from the rendering results that our CB-KNN method does not exhibit image blurring in both novel and training views. Compared with SplaTAM[10], our method achieves comparable fidelity to the ground truth in both color maps and depth maps rendered for novel and training views.

[9] Jürgen Sturm, Nikolas Engelhard, Felix Endres, Wolfram Burgard, and Daniel Cremers, “A benchmark for the evaluation of rgbd slam systems,” in *2012 IEEE/RSJ international conference on intelligent robots and systems*. IEEE, 2012, pp. 573–580.

[10] Nikhil Keetha, Jay Karhade, Krishna Murthy Jatavallabhula, Gengshan Yang, Sebastian Scherer, Deva Ramanan, and Jonathon Luiten, “Splatam: Splat track & map 3d gaussians for dense rgbd slam,” in *Proceedings of the IEEE/CVF Conference on Computer Vision and Pattern Recognition*, 2024, pp. 21357–21366.

[11] Carlos Campos, Richard Elvira, Juan J Gómez Rodríguez, José MM Montiel, and Juan D Tardós, “Orb-slam3: An accurate open-source library for visual, visual-inertial, and multimodal slam,” *IEEE transactions on robotics*, 2024.

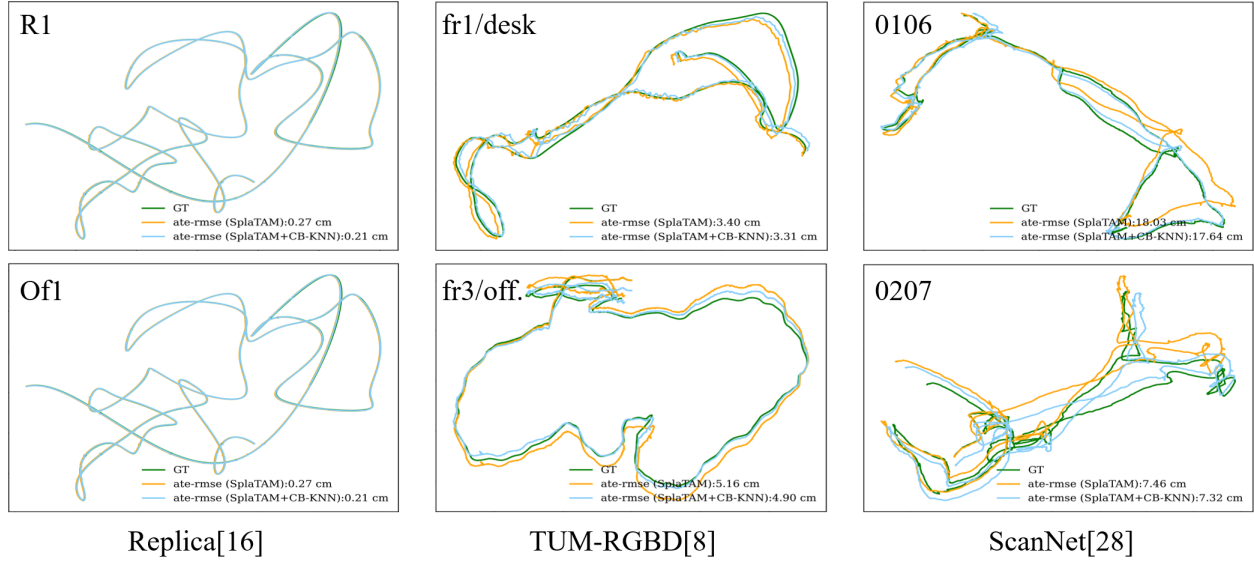


Fig. 4: Trajectory maps on Replica[16], TUM-RGBD[9], and ScanNet[45].

TABLE IV: Novel And Train View Rendering Performance on Replica/R0

Methods	Metrics	Novel View R0	Training View R0
SplatAM[10]	PSNR↑	31.94	32.87
	SSIM↑	0.98	0.99
	LPIPS↓	0.07	0.06
	Depth L1↓	0.52	0.49
Ours	PSNR↑	32.54	33.99
	SSIM↑	0.98	0.99
	LPIPS↓	0.06	0.04
	Depth L1↓	0.50	0.43

TABLE V: Runtime on Replica/R0 using a RTX A40.

Methods	Tracking /Iteration	Mapping /Iteration	Tracking /Frame	Mapping /Frame	ATE RMSE [cm]↓
SplatAM[10]	29ms	32ms	1.19s	2.26s	0.30cm
Ours	23ms	25ms	0.94s	1.75s	0.27cm

TABLE VI: FPS and Keyframe time when running on Replica/R0 with RTX A40.

Methods	FPS↑	Keyframe /time
SplatAM[10]	0.31	3.05ms
Ours	0.43	3.42ms

tions on robotics, vol. 37, no. 6, pp. 1874–1890, 2021.

[12] Jakob Engel, Vladlen Koltun, and Daniel Cremers, “Direct sparse odometry,” *IEEE transactions on pattern analysis and machine intelligence*, vol. 40, no. 3, pp. 611–625, 2017.

[13] Jakob Engel, Thomas Schöps, and Daniel Cremers, “Lsd-slam: Large-scale direct monocular slam,” in *European conference on computer vision*. Springer, 2014, pp. 834–849.

[14] Thomas Whelan, Stefan Leutenegger, Renato F Salas-Moreno, Ben Glocker, and Andrew J Davison, “Elasticfusion: Dense slam without a pose graph.,” in *Robotics: science and systems*. Rome, 2015, vol. 11.

[15] Oliver J Woodford and Edward Rosten, “Large scale photometric bundle adjustment,” *arXiv preprint arXiv:2008.11762*, 2020.

[16] Julian Straub, Thomas Whelan, Lingni Ma, Yufan Chen, Erik Wijmans, Simon Green, Jakob J Engel, Raul Mur-Artal, Carl Ren, Shobhit Verma, et al., “The replica dataset: A digital replica of indoor spaces,” *arXiv preprint arXiv:1906.05797*, 2019.

[17] Michael Burri, Janosch Nikolic, Pascal Gohl, Thomas Schneider, Joern Rehder, Sammy Omari, Markus W Achterlik, and Roland Siegwart, “The euroc micro aerial vehicle datasets,” *The International Journal of Robotics Research*, vol. 35, no. 10, pp. 1157–1163, 2016.

[18] Antoni Buades, Bartomeu Coll, and J-M Morel, “A non-local algorithm for image denoising,” in *2005 IEEE computer society conference on computer vision and pattern recognition (CVPR’05)*. Ieee, 2005, vol. 2, pp. 60–65.

[19] Wenjie Li, Jia Liu, Yanyan Wang, Wei Hao, Dayong Ren, and Lijun Chen, “Dl-posenet: A differential lightweight network for pose regression over se (3),” in *2024 IEEE International Conference on Robotics and Automation (ICRA)*. IEEE, 2024, pp. 16834–16840.

[20] Wenjie Li, Jia Liu, Wei Hao, Haisong Liu, Dayong Ren, Yanyan Wang, and Lijun Chen, “Online deep bingham network for probabilistic orientation estimation,” *IET Computer Vision*, vol. 17, no. 6, pp. 663–675, 2023.

[21] Shachar Fleishman, Daniel Cohen-Or, and Cláudio T Silva, “Robust moving least-squares fitting with sharp features,” *ACM transactions on graphics (TOG)*, vol. 24, no. 3, pp. 544–552, 2005.

[22] Yujing Sun, Scott Schaefer, and Wenping Wang, “Denoising point sets via lo minimization,” *Computer Aided Geometric Design*, vol. 35, pp. 2–15, 2015.

[23] Tino Werner, “Applications of robust statistics in autonomous driving,” 2025.

[24] Paul Bergmann, Rui Wang, and Daniel Cremers, “Online photometric calibration of auto exposure video for realtime visual odometry and slam,” *IEEE Robotics and Automation Letters*, vol. 3, no. 2, pp. 627–634, 2017.

[25] Oliver J Woodford and Edward Rosten, “Large scale photometric bundle adjustment,” *arXiv preprint arXiv:2008.11762*, 2020.

[26] Lei Cheng, Junpeng Hu, Haodong Yan, Mariia Gladkova, Tianyu Huang, Yun-Hui Liu, Daniel Cremers, and Haoang Li, “Physically-based photometric bundle adjustment in non-lambertian environments,” in *2024 IEEE/RSJ International Conference on Intelligent Robots and Systems (IROS)*. IEEE, 2024, pp. 10461–10468.

[27] Dayong Ren, Shuangyu Yang, Wenjie Li, Jie Guo, and Yanwen Guo, “Sae: Estimation for transition matrix in annotation algorithms,” *arXiv preprint*, 2022.

[28] Dayong Ren, Zhengyi Wu, Jiawei Li, Piaopiao Yu, Jie Guo, Mingqiang Wei, and Yanwen Guo, “Point attention network for point cloud semantic segmentation,” *Science China Information Sciences*, vol. 65, no. 9, pp. 192104, 2022.

[29] Dayong Ren, Zhe Ma, Yuanpei Chen, Weihang Peng, Xiaode Liu,

Yuhan Zhang, and Yufei Guo, "Spiking pointnet: Spiking neural networks for point clouds," *Advances in Neural Information Processing Systems*, vol. 36, 2024.

[30] Dayong Ren, Jiawei Li, Zhengyi Wu, Jie Guo, Mingqiang Wei, and Yanwen Guo, "Mffnet: multimodal feature fusion network for point cloud semantic segmentation," *The Visual Computer*, vol. 40, no. 8, pp. 5155–5167, 2024.

[31] Hengyi Wang, Jingwen Wang, and Lourdes Agapito, "Co-slam: Joint coordinate and sparse parametric encodings for neural real-time slam," in *Proceedings of the IEEE/CVF Conference on Computer Vision and Pattern Recognition*, 2023, pp. 13293–13302.

[32] Vladimir Yugay, Yue Li, Theo Gevers, and Martin R Oswald, "Gaussian-slam: Photo-realistic dense slam with gaussian splatting," *arXiv preprint arXiv:2312.10070*, 2023.

[33] Mohammad Mahdi Johari, Camilla Carta, and François Fleuret, "Es-lam: Efficient dense slam system based on hybrid representation of signed distance fields," in *Proceedings of the IEEE/CVF conference on computer vision and pattern recognition*, 2023, pp. 17408–17419.

[34] Erik Sandström, Yue Li, Luc Van Gool, and Martin R Oswald, "Point-slam: Dense neural point cloud-based slam," in *Proceedings of the IEEE/CVF International Conference on Computer Vision*, 2023, pp. 18433–18444.

[35] Zihan Zhu, Songyou Peng, Viktor Larsson, Weiwei Xu, Hujun Bao, Zhaopeng Cui, Martin R Oswald, and Marc Pollefeys, "Nice-slam: Neural implicit scalable encoding for slam," in *Proceedings of the IEEE/CVF conference on computer vision and pattern recognition*, 2022, pp. 12786–12796.

[36] Xingrui Yang, Hai Li, Hongjia Zhai, Yuhang Ming, Yuqian Liu, and Guofeng Zhang, "Vox-fusion: Dense tracking and mapping with voxel-based neural implicit representation," in *2022 IEEE International Symposium on Mixed and Augmented Reality (ISMAR)*. IEEE, 2022, pp. 499–507.

[37] Lipu Zhou, Shengze Wang, and Michael Kaess, "π-lsam: Lidar smoothing and mapping with planes," in *2021 IEEE international conference on robotics and automation (ICRA)*. IEEE, 2021, pp. 5751–5757.

[38] Yanwen Guo, Yuanqi Li, Dayong Ren, Xiaohong Zhang, Jiawei Li, Liang Pu, Changfeng Ma, Xiaoyu Zhan, Jie Guo, Mingqiang Wei, et al., "Lidar-net: A real-scanned 3d point cloud dataset for indoor scenes," in *Proceedings of the IEEE/CVF Conference on Computer Vision and Pattern Recognition*, 2024, pp. 21989–21999.

[39] Sensen Song, Dayong Ren, Zhenhong Jia, and Fei Shi, "Adaptive gaussian regularization constrained sparse subspace clustering for image segmentation," in *ICASSP 2024-2024 IEEE International Conference on Acoustics, Speech and Signal Processing (ICASSP)*. IEEE, 2024, pp. 4400–4404.

[40] Alexandru Brateanu, Raul Balmez, Adrian Avram, and Ciprian Orhei, "Akdt: Adaptive kernel dilation transformer for effective image denoising," *Proceedings Copyright*, vol. 418, no. 425, pp. 19.

[41] Lianchao Wang, Yijin Chen, Wenhui Song, and Hanghang Xu, "Point cloud denoising and feature preservation: an adaptive kernel approach based on local density and global statistics," *Sensors*, vol. 24, no. 6, pp. 1718, 2024.

[42] Chen Chen, Yisen Wang, Honghua Chen, Xuefeng Yan, Dayong Ren, Yanwen Guo, Haoran Xie, Fu Lee Wang, and Mingqiang Wei, "Geosegnet: point cloud semantic segmentation via geometric encoder–decoder modeling," *The Visual Computer*, vol. 40, no. 8, pp. 5107–5121, 2024.

[43] Linshuang Diao, Dayong Ren, Sensen Song, and Yurong Qian, "Zigzagpointmamba: Spatial-semantic mamba for point cloud understanding," *arXiv preprint arXiv:2505.21381*, 2025.

[44] Dayong Ren, Zhenhong Jia, Jie Yang, and Nikola K Kasabov, "A practical grabcut color image segmentation based on bayes classification and simple linear iterative clustering," *IEEE Access*, vol. 5, pp. 18480–18487, 2017.

[45] Angela Dai, Angel X Chang, Manolis Savva, Maciej Halber, Thomas Funkhouser, and Matthias Nießner, "Scannet: Richly-annotated 3d reconstructions of indoor scenes," in *Proceedings of the IEEE conference on computer vision and pattern recognition*, 2017, pp. 5828–5839.